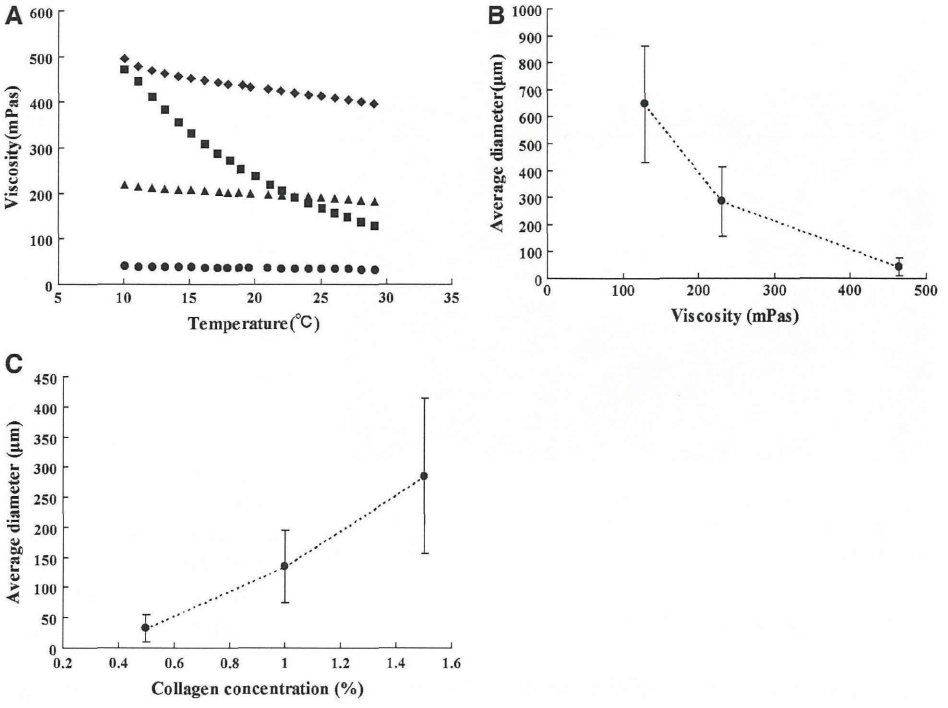

Fig. 3 **a** Effect of reaction temperature on the viscosities of liquid paraffin (*squares*), 0.5% collagen (*circles*), 1.0% collagen (*triangles*), and 1.5% collagen solutions (*diamonds*), respectively. **b** Effect of viscosity in oil-phase on particle diameters. **c** Effect of collagen concentration in water-phase on particle diameters. Surfactant concentration and rotating speed were set to 0.1% and 500 rpm, respectively

should be controlled to make the collagen microspheres having intended particle diameters.

3.4 Zeta potential

The surface charge of the collagen microspheres was determined by measuring their electrophoretic mobility. Table 3 shows the zeta potential values of the collagen microspheres in PBS and EGM. The collagen microspheres in the present study had slight positive charge. Berthold et al. [8] have reported that marine collagen microspheres showed negative charge of about −30 mV at pH 7. The difference could be caused by the types of crosslinking agents used. The present study used WSC, which forms crosslinks between amino groups and carboxyl groups by condensation reaction [14]. On the other hand, previous reports used glutaraldehyde, which forms crosslinks between only amino groups and has some incomplete reaction of the bifunctional reagent leading to free aldehyde groups [8]. Therefore, the charge distribution of the functional groups in collagen molecules might cause the difference in the zeta potential compared to the previous studies. Meanwhile, the zeta potential in EGM was slightly lower than that in PBS. It has been reported that the electrostatic binding of buffer anions to the surface of the positively charged microspheres could be observed [15, 16]. Therefore, the difference in the concentration of buffer anions and ionic strength between PBS and EGM might influence the zeta potential.

3.5 SEM and SDS-PAGE

SEM photographs show spherical particles with a smooth surface and a diameter of ca. 2.5 μm (Fig. 4). Some of the particles were found to be aggregated (data now shown). Low zeta potential of the collagen microspheres could lead the aggregation due to the interparticle attraction forces such as van der Waals' force. We performed the SDS-PAGE analysis to prove that the microspheres were indeed collagen and not denatured, but could not see any bands of collagen as well as those of gelatin (data not shown), indicating that the chemical crosslinks between collagen molecules made it difficult to denature the collagen microspheres by heat. Our previous experiments have demonstrated that the collagen sponge crosslinked with WSC had over 100°C of denaturation peak in differential scanning calorimeter analysis (unpublished data), which may explain the SDS-PAGE results. Raman spectroscopy and Fourier transform infrared spectroscopy are needed to prove the collagen denaturation in future works.

Table 3 Zeta potential values of collagen microspheres in PBS and EGM

Solvents	Zeta potential (mV)
PBS	8.86 ± 0.30
EGM	3.15 ± 0.63

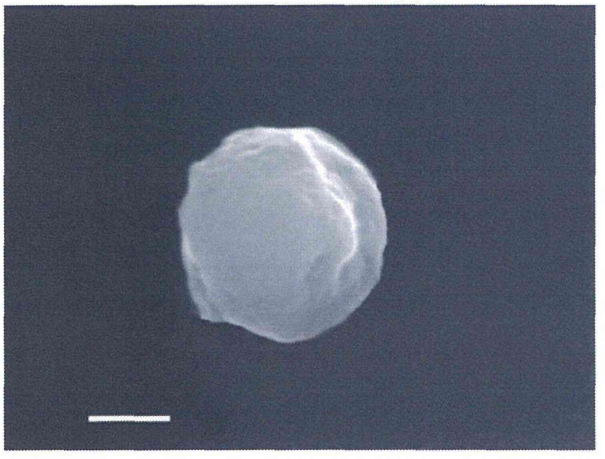

Fig. 4 SEM photograph of collagen microspheres. The microspheres were prepared under conditions of rotating speed of 600 rpm and surfactant concentration of 0.3%. Magnification: ×15,000. Bar: 1 μm

3.6 Release profile of rhVEGF

The release profile of rhVEGF from the collagen microspheres was different among the solvents used (Fig. 5a). In the case of collagenase solution, the rhVEGF released with a rapid rate during initial 8 days, followed by a slower release rate for the remaining duration of the experiment.

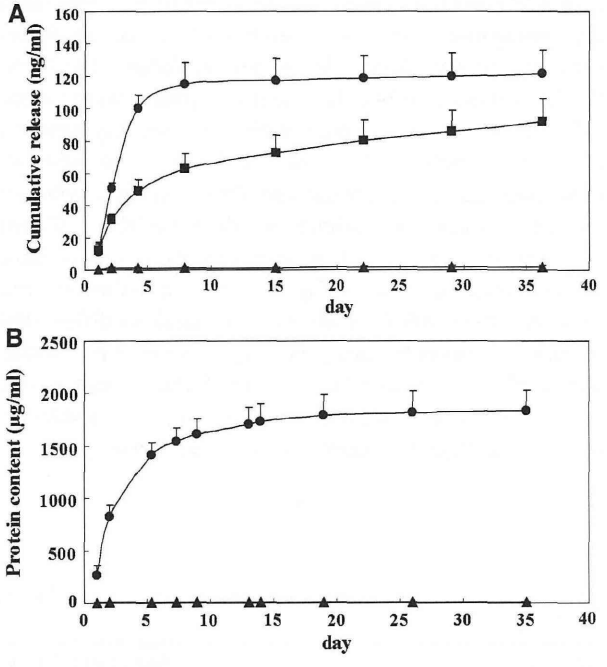

Fig. 5 **a** In vitro release profile of rhVEGF-loaded collagen microspheres in collagenase solution (*circles*), PBS (*triangles*), and EGM (*squares*). **b** In vitro degradation rate of collagen microspheres in collagenase solution (*circles*) and PBS (*triangles*)

The release curve in collagenase solution was similar to the degradation curve of the collagen microspheres in collagenase solution (Fig. 5b), indicating that the drug release could occur by degradation of the collagen microspheres. The collagenase concentration (1 U/ml) used in this study was in the physiologically relevant concentration range [17], therefore, the collagen microspheres might show the same release profile as the collagenase solution results. Meanwhile, the release rate into EGM was higher than that into PBS, indicating that drug diffusion between EGM and PBS could be occurred. Additionally, the difference in the charge state of the collagen microspheres in the solvents might affect the release rate (Table 3). It is believed that there are binding forces, such as electrostatic and hydrophobic interactions, between collagen and protein [18]. Therefore, the change in the electrostatic interaction between the collagen microspheres and rhVEGF might be one of the reasons for the difference in the release profile. Consequently, rhVEGF could be released by drug diffusion as well as collagen degradation.

3.7 Bioactivity of released rhVEGF

An in vitro capillary formation assay was performed to evaluate whether the released rhVEGF remained bioactive (Fig. 6). We have reported that the HUVECs co-cultured on NHDFs showed capillary-like structures in the presence of VEGF in the EGM [13]. The HUVECs co-cultured on NHDFs were exposed to the conditioned EGM which were collected after incubation with rhVEGF-loaded collagen microspheres for 0–7, 8–14, 15–21, and 22–28 days. Cells treated with the conditioned EGM showed capillary formation although the total length of the capillary was small compared to the control from the area calculation results using a software analysis (data not shown) and became smaller with increasing incubation periods. This can be explained from the release profile results of EGM (Fig. 4a, squares); the release amount of rhVEGF in EGM became lower with increasing incubation periods. The total amounts of rhVEGF released at 0–7, 8–14, 15–21, and 22–28 days were 56.5, 15.0, 8.8, and 6.2 ng/ml, respectively, which were lower than the control (76.4 ng/ml). Consequently, the bioactivity of rhVEGF was maintained after release as observed capillary formation.

There are some reports to make collagen microspheres for tissue engineering. Kim et al. [6] reported the collagen-apatite composite microspheres for bone tissue engineering with average diameter of 166 μm. Swatschek et al. [19] reported the agglomated collagen microspheres for retinol delivery with average diameter of 2.2 μm. Berthold et al. [8] reported the collagen microspheres for glucocorticosteroids delivery with average diameter of 10 μm. Recently, Chan et al. [20] reported the nano-

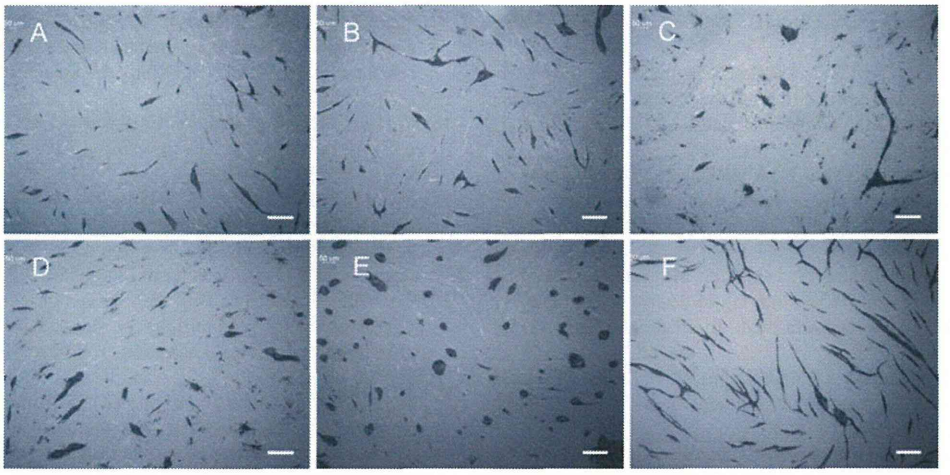

Fig. 6 Capillary forming ability of HUVECs cultured in conditioned EGM which were collected after incubation with rhVEGF-loaded collagen microspheres for 0–7 days (**a**), 8–14 days (**b**), 15–21 days (**c**), and 22–28 days (**d**). Controls were untreated cells (**e**) and the cells treated with EGM containing 2 nM rhVEGF (**f**), respectively. Bars: 100 μm

fibrous collagen microspheres with average diameter of 70 μm and demonstrated their release profiles of nerve growth factor. The present study demonstrated smaller collagen microspheres having 1–30 μm diameters and the release profile of bioactive rhVEGF during 4 weeks incubation. Additionally, the present study first provides the technique for easy control of particle diameter of collagen microspheres. Crosslinker WSC used in this study is known to be biocompatible because WSC do not persist in the linkage between collagen molecules and are simply washed away after crosslinking [21]. Consequently, the collagen microspheres have potential use for clinical applications, such as injectable DDS biomaterials for tissue engineering.

4 Conclusions

We successfully fabricated the collagen microspheres for sustained release of rhVEGF. The particle size can be easily controlled by changing surfactant concentrations and rotating speeds in the process of emulsification. The sustained release of rhVEGF was achieved for 4 weeks and the released rhVEGF remained bioactive. This work contributes to future development of collagen microsphere-based protein delivery system for tissue engineering.

Acknowledgments This work was supported by Takeda Science Foundation and the Research for Promoting Technological Seeds from Japan Science and Technology Agency. We thank Shunji Yunoki PhD, Risa Itoh and Masanobu Munekata PhD, Hokkaido University, for helpful advices and technical assistances. We thank Sysmex for measurements of zeta potential and helpful advices.

References

1. Cross MJ, Claesson-Welsh L. FGF and VEGF function in angiogenesis: signalling pathways, biological responses and therapeutic inhibition. Trends Pharmacol Sci. 2001;22(4):201–7.
2. Morishita M, Peppas NA. Is the oral route possible for peptide and protein drug delivery? Drug Discov Today. 2006;11(19–20):905–10.
3. De la Riva B, Nowak C, Sanchez E, Hernandez A, Schulz-Siegmund M, Pec MK, et al. VEGF-controlled release within a bone defect from alginate/chitosan/PLA-H scaffolds. Eur J Pharm Biopharm. 2009;73(1):50–8.
4. Lee J, Lee KY. Local and sustained vascular endothelial growth factor delivery for angiogenesis using an injectable system. Pharm Res. 2009;26(7):1739–44.
5. Bagal A, Dahiya R, Tsai V, Adamson PA. Clinical experience with polymethylmethacrylate microspheres (Artecoll) for soft-tissue augmentation: a retrospective review. Arch Facial Plast Surg. 2007;9(4):275–80.
6. Kim HW, Gu HJ, Lee HH. Microspheres of collagen-apatite nanocomposites with osteogenic potential for tissue engineering. Tissue Eng. 2007;13(5):965–73.
7. Kim SS, Gwak SJ, Choi CY, Kim BS. Skin regeneration using keratinocytes and dermal fibroblasts cultured on biodegradable microspherical polymer scaffolds. J Biomed Mater Res B Appl Biomater. 2005;75(2):369–77.
8. Berthold A, Cremer K, Kreuter J. Collagen microparticles: carriers for glucocorticosteroids. Eur J Pharm Biopharm. 1998;45(1):23–9.
9. Hwang SM, Kim DD, Chung SJ, Shim CK. Delivery of ofloxacin to the lung and alveolar macrophages via hyaluronan microspheres for the treatment of tuberculosis. J Control Release. 2008;129(2):100–6.
10. Mathew ST, Devi SG, Kv S. Formulation and evaluation of ketorolac tromethamine-loaded albumin microspheres for potential intramuscular administration. AAPS PharmSciTech. 2007;8(1):14.
11. Wei HJ, Yang HH, Chen CH, Lin WW, Chen SC, Lai PH, et al. Gelatin microspheres encapsulated with a nonpeptide angiogenic agent, ginsenoside Rg1, for intramyocardial injection in a rat

model with infarcted myocardium. J Control Release. 2007; 120(1–2):27–34.
12. Nagai N, Yunoki S, Suzuki T, Sakata M, Tajima K, Munekata M. Application of cross-linked salmon atelocollagen to the scaffold of human periodontal ligament cells. J Biosci Bioeng. 2004;97(6):389–94.
13. Nagai N, Hirakawa A, Otani N, Munekata M. Development of tissue-engineered human periodontal ligament constructs with intrinsic angiogenic potential. Cells Tissues Organs. 2009; 190(6):303–12.
14. Olde Damink LH, Dijkstra PJ, van Luyn MJ, van Wachem PB, Nieuwenhuis P, Feijen J. Cross-linking of dermal sheep collagen using a water-soluble carbodiimide. Biomaterials. 1996;17(8): 765–73.
15. Kosmulski M, Prochniak P, Rosenholm JB. Solvents, in which ionic surfactants do not affect the zeta potential. J Colloid Interface Sci. 2010;342(1):110–3.
16. Sethi M, Joung G, Knecht MR. Stability and electrostatic assembly of au nanorods for use in biological assays. Langmuir. 2009;25(1):317–25.
17. Yao C, Roderfeld M, Rath T, Roeb E, Bernhagen J, Steffens G. The impact of proteinase-induced matrix degradation on the release of VEGF from heparinized collagen matrices. Biomaterials. 2006;27(8):1608–16.
18. Wallace DG, Rosenblatt J. Collagen gel systems for sustained delivery and tissue engineering. Adv Drug Deliv Rev. 2003;55(12):1631–49.
19. Swatschek D, Schatton W, Muller W, Kreuter J. Microparticles derived from marine sponge collagen (SCMPs): preparation, characterization and suitability for dermal delivery of all-trans retinol. Eur J Pharm Biopharm. 2002;54(2):125–33.
20. Chan OC, So KF, Chan BP. Fabrication of nano-fibrous collagen microspheres for protein delivery and effects of photochemical crosslinking on release kinetics. J Control Release. 2008;129 (2):135–43.
21. Nagai N, Nakayama Y, Zhou YM, Takamizawa K, Mori K, Munekata M. Development of salmon collagen vascular graft: mechanical and biological properties and preliminary implantation study. J Biomed Mater Res B Appl Biomater. 2008;87(2): 432–9.

平成24年度

OPEN ACCESS Freely available online

PLOS ONE

Transscleral Sustained Vasohibin-1 Delivery by a Novel Device Suppressed Experimentally-Induced Choroidal Neovascularization

Hideyuki Onami[1,2☯], Nobuhiro Nagai[1☯], Hirokazu Kaji[3], Matsuhiko Nishizawa[3], Yasufumi Sato[4], Noriko Osumi[5], Toru Nakazawa[2], Toshiaki Abe[1*]

1 Division of Clinical Cell Therapy, United Centers for Advanced Research and Translational Medicine (ART), Tohoku University Graduate School of Medicine, Sendai, Japan, **2** Department of Ophthalmology, Tohoku University Graduate School of Medicine, Sendai, Japan, **3** Department of Bioengineering and Robotics, Graduate School of Engineering, Tohoku University, Sendai, Japan, **4** Department of Vascular Biology, Institute of Development, Aging and Cancer, Tohoku University, Sendai, Japan, **5** Division of Developmental Neuroscience, United Centers for Advanced Research and Translational Medicine (ART), Tohoku University Graduate School of Medicine, Sendai, Japan

Abstract

We established a sustained vasohibin-1 (a 42-kDa protein), delivery device by a novel method using photopolymerization of a mixture of polyethylene glycol dimethacrylate, triethylene glycol dimethacrylate, and collagen microparticles. We evaluated its effects in a model of rat laser-induced choroidal neovascularization (CNV) using a transscleral approach. We used variable concentrations of vasohibin-1 in the devices, and used an enzyme-linked immunosorbent assay and Western blotting to measure the released vasohibin-1 (0.31 nM/day when using the 10 μM vasohibin-1 delivery device [10VDD]). The released vasohibin-1 showed suppression activity comparable to native effects when evaluated using endothelial tube formation. We also used pelletized vasohibin-1 and fluorescein isothiocyanate-labeled 40 kDa dextran as controls. Strong fluorescein staining was observed on the sclera when the device was used for drug delivery, whereas pellet use produced strong staining in the conjunctiva and surrounding tissue, but not on the sclera. Vasohibin-1 was found in the sclera, choroid, retinal pigment epithelium (RPE), and neural retina after device implantation. Stronger immunoreactivity at the RPE and ganglion cell layers was observed than in other retinal regions. Significantly lower fluorescein angiography (FA) scores and smaller CNV areas in the flat mounts of RPE-choroid-sclera were observed for the 10VDD, VDD (1 μM vasohibin-1 delivery device), and vasohibin-1 intravitreal direct injection (0.24 μM) groups when compared to the pellet, non-vasohibin-1 delivery device, and intravitreal vehicle injection groups. Choroidal neovascularization can be treated with transscleral sustained protein delivery using our novel device. We offer a safer sustained protein release for treatment of retinal disease using the transscleral approach.

Citation: Onami H, Nagai N, Kaji H, Nishizawa M, Sato Y, et al. (2013) Transscleral Sustained Vasohibin-1 Delivery by a Novel Device Suppressed Experimentally-Induced Choroidal Neovascularization. PLoS ONE 8(3): e58580. doi:10.1371/journal.pone.0058580

Editor: Olaf Strauß, Eye Hospital, Charité, Germany

Received August 11, 2012; **Accepted** February 6, 2013; **Published** March 5, 2013

Funding: This work was supported in part by Grant-in-Aid for Scientific Research (No. 21592214) and Young Scientists (A) (No. 23680054) from the Ministry of Education, Culture, Sports, Science, and Technology, Health Labour Sciences Research Grant from the Ministry of Health Labour and Welfare (No. H23-iryokiki-wakate-003, H23-kankaku-ippan-004, H24-nanchitoh-ippan-067), the Suzuken Memorial Foundation, and the Ichiro Kanehara Foundation. The funders had no role in study design, data collection and analysis, decision to publish, or preparation of the manuscript.

Competing Interests: The authors have declared that no competing interests exist.

* E-mail: toshi@oph.med.tohoku.ac.jp

☯ These authors contributed equally to this work.

Introduction

Age-related macular degeneration (AMD) is a well-known sight-threatening disease in developed countries [1]. Although many treatment regimens have been used to treat AMD [2–6], intravitreal injection of anti-vascular endothelial growth factor (VEGF) produced lesion improvement and better visual acuity in some patients [7,8]. However, intra-vitreal injection of anti-VEGF also produced irritation, infection, and other adverse side effects [9]. Further, that treatment required repeated injections, usually occurring once a month [7,8]. Thus, other types of drugs or drug delivery systems (DDSs) need to be developed to treat AMD.

Eye drops and systemic drug administration are unsuitable for retinal diseases if the physician is looking for effective drug penetration into the eye, especially for macular diseases such as AMD [10,11]. Although drug delivery device implantation into the vitreous showed effective delivery of drug to the retina, these treatments may cause severe side effects, such as infection, vitreous hemorrhage, or retinal detachment [12–14]. Drug delivery using viral vectors has been attempted for treatment of devastating retinal diseases [15]; however, this method may induce immune cell or humoral responses [16,17].

Subconjunctival drug delivery is less invasive than intravitreal drug injection and can deliver more drug than seen with eye drops or systemic administration [10,11]. There are published data investigating clinical use of subconjunctival drug administration [18,19]. Thus, the subconjunctival route may be an attractive method for drug delivery to the retina. The major difficulties with subconjunctival DDS are uncontrollable release of the target drug [20], as well as an unknown drug delivery route and mechanism to

reach the retina [20,21]. Sustained release, with no drug bolus effect, would be required to reduce side effects [22,23].

We previously reported our results of the use of a novel drug delivery device placed on the sclera that we thought would be an effective tool in treating retinal diseases [24]. The device consisted of a drug-releasing semi-permeable membrane and impermeable membranes acting as the drug reservoir. Because of the non-biodegradable and one-way release nature of the device, we could achieve sustained release of the drug to the retina. We examined the effects of this device using a laser-induced choroidal neovascularization (CNV) model in rats.

Anti-VEGF antibody is a well-known treatment agent in CNV therapy, but suppression of VEGF function may induce many harmful effects in physiological function [25]. We selected vasohibin-1 for the loading drug in the device in this study because of its well-known anti-angiogenic activity [26,27]. Vasohibin-1 is a 42-kDa polypeptide, a VEGF-inducible molecule expressed by cultured human endothelial cells (ECs) [26]. Vasohibin-1 inhibits the formation of EC networks *in vitro*, corneal neovascularization *in vitro* [26], retinal neovascularization in a mouse model of oxygen-induced ischemic retinopathy [27], and laser-induced mouse [25] and monkey CNV [28]. Each of the *in vivo* studies treated the tissue by direct intravitreal injection of vasohibin-1.

Here we shall show that continuous trans-scleral vasohibin-1 delivery by the device can suppress laser-induced CNV in rat eyes (Fig. 1A) as well as that by intravitreal injection. This technique and device may hold promise for safer and more effective treatment of patients with AMD.

Methods

Vasohibin-1 and Device Preparation

Vasohibin-1 was purified as reported previously [25]. For the preparation of the vasohibin-1 formulation, an 80-μL volume of vasohibin-1 (either 1.25 or 12.5 μM) in vehicle (phosphate buffered saline [PBS] control) was mixed with 20 μL of polyethylene glycol dimethacrylate (PEGDM), then underwent UV curing at an intensity of 11.5 mJ/cm^2 (Lightningcure LCS; Hamamatsu Photonics, Hamamatsu City, Japan) for 3 minutes.

The devices consisted of a semi-permeable drug-releasing membrane and an impermeable reservoir (Fig. 1A, 1B), as we reported previously [24]. The loaded vasohibin-1 doses included vehicle only (identified as NVDD), 1 μM vasohibin-1 (VDD), and 10 μM vasohibin-1 (10VDD), with a total volume of 1.5 μL in each device. The size of the device was 2 mm×2 mm wide ×1 mm high (drug-releasing surface area; 1.5 mm×1.5 mm = 2.25 mm^2) for the rat experiments (Fig. 1B, device) and 4 mm×4 mm×1.5 mm (drug-releasing surface area; 3.5 mm×3.5 mm = 12.25 mm^2) for the vasohibin-1 releasing *in vitro* assay. The release amount from the transplanted device was small and it was very difficult to detect released vasohibin-1 by the standard ELISA technique, so we decided to use a larger device for the ELISA procedure. As a control, we used pelletized vasohibin-1 without the reservoir and permeable membrane (Fig. 1B, pellet). The concentration of pelletized vasohibin-1 was adjusted to be the same concentration as that of the 10VDD (10 μM vasohibin-1). The total amount of vasohibin-1 released from the 10VDD device during the 2-week *in vivo* experiment was aimed to be equivalent to that of the intravitreal vasohibin-1 injection. A FITC-labeled 40 kDa dextran-loaded device (FD40DD) was also used for monitoring the position of the implanted device.

In Vitro Experiments

***1 In Vitro* Release Assay, Enzyme-linked Immunosorbent Assay, and Western Blotting.** The devices loaded with vasohibin-1 were placed in the wells of a 24-well culture plate filled with 200 μL PBS at 37°C. Aliquots (200 μL) of the buffer in each well were collected at Days 1, 7, 14, and 28 during change-out of old buffer for new buffer solution. The collected samples were considered to include only protein for vasohibin-1. We then determined the amount of vasohibin-1 in the buffer using an enzyme-linked immunosorbent assay (ELISA) [29] and western blotting [30]. The intensity of the color of the ELISA reaction products was measured with a microplate reader (MAXline; Molecular Devices Corporation, Sunnyvale, CA, USA). The measurements were made in duplicate, and the mean value was used for comparisons. The 50-μL collected samples and 100 fmol of recombinant vasohibin-1 (positive control) were loaded, separated by sodium dodecyl sulfate-polyacrylamide gel electrophoresis (SDS-PAGE) on a 10% separating gel, and transferred to nitrocellulose membranes for western blotting. The membranes were blocked for 1 hour at room temperature with 5% ECL blocking agent (GE Healthcare Biosciences, Pittsburgh, PA, USA), and then incubated overnight at 4°C in PBS containing 0.05% Tween 20 (T-PBS), 2.5% skim milk, and 1 μg/mL horseradish peroxidase-conjugated anti–vasohibin-1 monoclonal antibody. The membrane filters were washed 3 times with T-TBS and the blots were detected using an enhanced chemiluminescence method (ECL Western Blotting Detection Kit; Amersham Biosciences, Piscataway, NJ, USA). The results were visualized using an imaging system (ImageQuant LAS-1000; GE Healthcare Biosciences).

2 Endothelial Tube Formation. Endothelial tube formation was assessed with normal human umbilical vein endothelial cells (HUVECs) (Takara Bio; Otsu, Japan) co-cultured on neonatal normal human dermal fibroblasts (NHDF, Takara Bio) layer using anti-human CD31 immunostaining, as reported previously [28]. Two nM vascular endothelial growth factor (VEGF, Wako; Tokyo, Japan) was then added to the endothelial cell growth medium (EGM, Takara Bio) containing no vasohibin-1 (control), and 0.2, 2, or 10 nM vasohibin-1, respectively. VEGF (2 nM) and samples of vasohibin-1 released from the vasohibin-1-loaded device over 3 hours at 37°C were used to examine released vasohibin-1 activity. We collected the released vasohibin-1 from the pellet and used it at a concentration of 0.56 nM (as measured by ELISA). On Day 3, the cells were fixed and stained using an anti-human CD31 immunostaining kit (Kurabo; Tokyo, Japan) according to the manufacturer's instructions. The number of stained HUVECs was determined using a computerized system (Kurabo Angiogenesis Image Analyzer program; Kurabo).

In Vivo CNV Experiments

1 Animals. The procedures used in the animal experiments followed the guidelines of the Association for Research in Vision and Ophthalmology Statement for the Use of Animals in Ophthalmic and Vision Research, and they were approved by the Animal Care Committee of Tohoku University Graduate School of Medicine (Permit Number: 2011–136). Twenty Sprague-Dawley (SD) rats (Experiments 1 and 2) and 36 Brown Norway (BN) rats (Experiment 3) weighing between 250 and 300 g were used (Table 1). All animals were followed up to 2 weeks after device transplantation and/or laser burn. We examined the effects of devices either at 1 week or 2 weeks for FA evaluation and 2 weeks for flat-mount evaluation. Macro examination was performed at 1 and 2 weeks after the device transplantation. For all procedures, the rats were anesthetized with an intramuscular

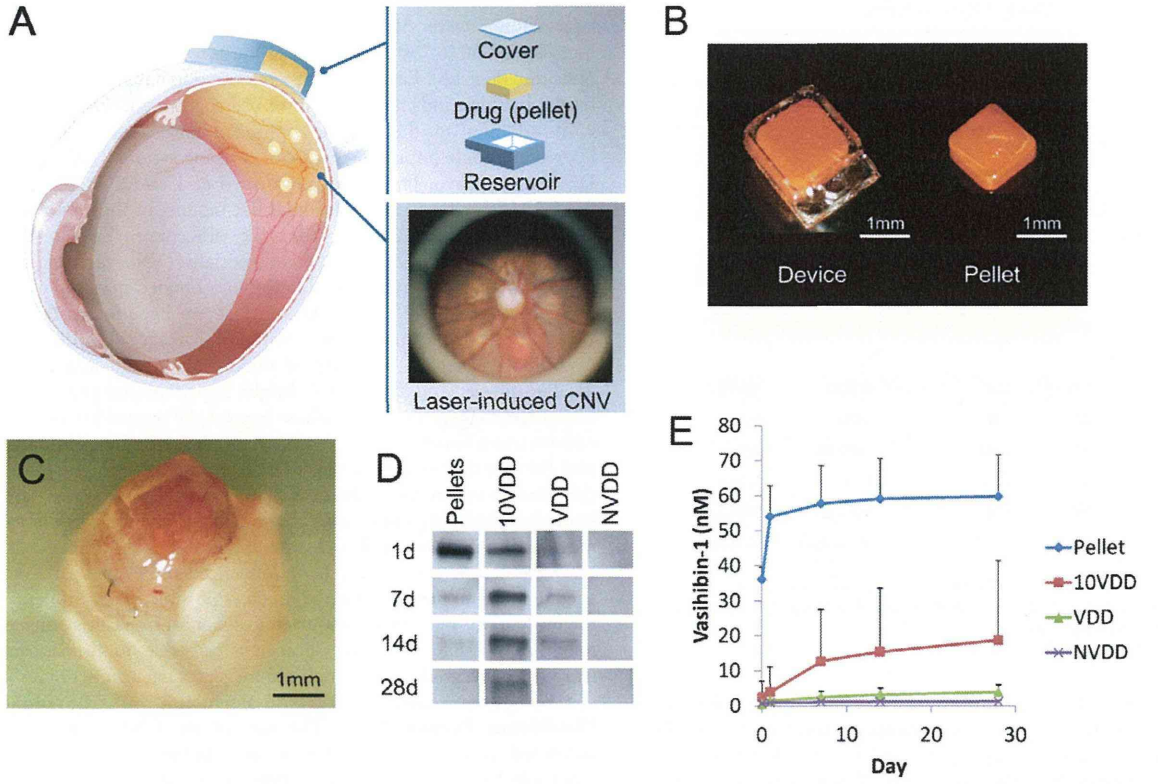

Figure 1. Device and vasohibin-1 release. (A) Schematic image of transscleral sustained vasohibin-1 delivery. We evaluated its effects via transscleral approach for rat laser-induced choroidal neovascularization (CNV). The device consists of a drug pelletized with PEGDM, a reservoir made of TEGDM, and a controlled-release membrane made of PEGDM that contains collagen microparticles. (B) Photograph showing a drug pellet and the delivery device containing a drug pellet. (C) Image of a device placed on the sclera of a rat eye at 3 days after implantation. The amount of vasohibin-1 in the PBS was measured at 1, 7, 14, and 28 days after starting incubation. The representative results of western blotting and the result of ELISA are shown in (D) and (E), respectively. We collected the samples at only the given time points and replaced only the equal volume of PBS. The released vasohibin-1 amounts accumulated for 6, 7, and 14 days. [The pellet samples collected at Day 1 (shown as 1d) were diluted five times due to their concentration before they were evaluated by western blotting]. NVDD: non-vasohibin-1 (vehicle) delivery device, VDD: 1 μM vasohibin-1 delivery device, 10VDD: 10 μM vasohibin-1 delivery device, Pellets: vasohibin-1 pelletized at the same concentration of 10VDD (without reservoir and cover).
doi:10.1371/journal.pone.0058580.g001

injection of ketamine hydrochloride (35 mg/kg) and xylazine hydrochloride (5 mg/kg), and the animals' pupils were dilated with topical 2.5% phenylephrine and 1% tropicamide. Oxybuprocaine hydrochloride (0.4%) was also used for local anesthesia. In all *in vivo* experiments, the animal's left eye was used as a control.

2 Implantation of VDDs, Pellets, and Intravitreal Vasohibin-1 Injection. Devices were implanted subconjunctively in the right eyes of the rats (Table 1). A 4-mm long conjunctival incision was made along the limbus in the upper temporal position. The devices were inserted into the subconjunctival space using forceps, with the drug-releasing surface facing the sclera. The device was placed between the optic disc and the equator, in the posterior quadrant, using no suture to anchor it into place. The conjunctival incision was closed with 9–0 silk and antibiotic ointment was applied to the eyes. Vasohibin-1 protein (0.24 μM) was injected using a 10-μL glass syringe (Hamilton; Reno, NV) 4 days after the experimental CNV procedure. The left eyes were used as untreated controls.

The rats were anesthetized, pupils were dilated, and a fundus examination was performed immediately after the surgery.

Experiment 1: Monitoring the Implanted Devices and Pellets

To monitor the device and drug release, fluorescein isothiocyanate (FITC) dextran (FD40; Sigma-Aldrich) pelletized with PEGDM was prepared and used as a control drug. The FD40 was dissolved in PBS at a concentration of 250 mg/mL and loaded in the device in the same way as vasohibin-1. Eight SD rats were included in this experiment; 4 rats received the FD40 delivery device (FD40DD) and 4 rats received only pelletized FD40.

Experiment 2: Immunohistochemistry after Device Implantation

Immunostaining for vasohibin-1was performed 2 weeks after device implantation. Twelve SD rats were used as follows (Table 1): 4 rats received vehicle (non-vasohibin-1) in the delivery device on the sclera (NVDD), 4 rats received 1.5 μL of 10 μM vasohibin-1 in the delivery device (10VDD), and 4 rats received 1.5 μL of 10 μM vasohibin-1 pellets implanted on the sclera. Immunohistochemistry was performed as reported previously [25].

Animals were euthanized using overdoses of ketamine hydrochloride and xylazine hydrochloride. The eyes were enucleated

Table 1. In Vivo Study Demographics.

Number of animals	Strain	Treatment	Methods	Position of implant
Experiment 1				
4	SD	Untreated	FD40DD	Sclera
4	SD	Untreated	FD40 Pellet	Sclera
Experiment 2				
4	SD	Untreated	NVDD	Sclera
4	SD	Untreated	10VDD	Sclera
4	SD	Untreated	Pellet	Sclera
Experiment 3				
6	BD	CNV	NVDD	Sclera
6	BD	CNV	VDD	Sclera
6	BD	CNV	10VDD	Sclera
6	BD	CNV	Pellet	Sclera
6	BD	CNV	Vehicle	Vitreous
6	BD	CNV	Vasohibin-1	Vitreous

SD: Sprague-Dawley rats, BN: Brown Norway rats, CNV: choroidal neovascularization, NVDD: non-vasohibin-1 delivery device, 10VDD: 10 μM vasohibin-1 delivery device.
doi:10.1371/journal.pone.0058580.t001

and fixed for 12 hours in 4% paraformaldehyde (PFA) at 4°C. The anterior segment and lens were removed from each eye. The posterior segment was cryoprotected at 4°C through successive 12-hour incubations in 10%, 20%, and 30% sucrose dissolved in saline. The tissues were immersed in OCT compound (Tissue-Tec; Sakura Finetec USA, Inc., Torrance, CA, USA) and frozen in acetone in a dry-ice bath. The frozen posterior segment was sectioned at the center of the implanted area at a thickness of 5 μm for each section, using a cryostat. We examined eight continuous sections per eye. The sections were incubated in rabbit polyclonal antibody against human vasohibin-1, followed by FITC-conjugated anti-rabbit IgG (1:200; Dako, Glostrup, Denmark) for 30 minutes. The sections were washed three times with PBS between each step. Negative controls (4 rats) incubated with just FITC-conjugated anti-rabbit IgG were also prepared. Slides were counterstained with 4, 6-diamino-1-phenylindole (DAPI; Vector Laboratories, Burlingame, CA, USA) and photographed using a fluorescence microscope (Leica FW4000, Ver. 1.2.1; Leica Microsystems Japan, Tokyo, Japan).

Experiment 3: Choroidal Neovascularization Study

A total of 36 BN rats were used (Table 1). The devices and pellets were implanted on the same day as the CNV procedure. The rats were divided into six groups (6 rats in each group): rats with NVDD, rats with 1.5 μL of 1 μM vasohibin-1 in the delivery device (VDD), rats with 1.5 μL of 10 μM vasohibin-1 in the delivery device (10VDD), rats with 1.5 μL of 10 μM vasohibin-1 pellets implanted on the sclera, rats with intravitreal injection of 5 μL of vehicle, and rats with an intravitreal injection of 0.24 μM vasohibin-1 protein occurring 4 days after the experimental CNV procedure. The amount of intravitreal vasohibin-1 used and the day of the injection were determined based on our previous data [25]. The intravitreal injections were performed using a 10-μL glass syringe (Hamilton), and the needle was passed through the sclera just behind the limbus into the vitreous cavity.

3 CNV procedure. A green argon laser was used to rupture the choroidal membrane using a slit-lamp delivery system (Ultima 2000SE; Lumenis, Yokneam, Israel) with a contact lens [31]. The laser settings were: 50 μm diameter for 0.1 sec duration, at an intensity of 650 to 750 mW. Six laser burns were made around the optic disc (Fig. 1A). Each burn was confirmed to have induced sub-retinal bubbles, indicating a rupture of Bruch's membrane.

In addition to the routine ophthalmological examinations, fluorescein angiography (FA) with an imaging system (GENESIS-Df; Kowa, Tokyo, Japan) was performed at 1 and 2 weeks after the CNV laser burn, and choroidal flat mounts of the CNV site were performed at 2 weeks after the procedure. Two retinal specialists (HO and TA) and one non-specialist (NN) evaluated the angiograms for FA grading evaluation in a blinded manner using a grading system [32], where Grade 1 = no hyperfluorescence; Grade 2 = hyperfluorescence without leakage; Grade 3 = hyperfluorescence in the early or middle phase and leakage in the late phase; and Grade 4 = bright hyperfluorescence in the transit and leakage in the late phase beyond the treated areas. The camera was a handheld retinal camera for photographing humans, and the fact that rat eye optics differ from that of humans made the process somewhat difficult. Intense fluorescein leakage also made the results of photographs as faint. The laser burn sometimes made subretinal hemorrhages that were shown as fluorescein blockage. These results may have influenced the evaluation. We tried to focus on the laser burn as much as possible to not influence the evaluation. Further we also tried to synchronize evaluations as much as possible to avoid significant bias due to fluorescein leakage. Total grades were analyzed for statistical significance.

4 Fluorescein-Labeled Dextran Perfusion and Choroidal Flat-Mount Preparation. The size of the CNV lesion was measured on choroidal flat mounts to examine the effect of the vasohibin-1 delivery device (n = 6 eyes/group and each eye had 6 laser spots). Fourteen days after the CNV procedure, the rats were perfused with 5 mL PBS containing 50 mg/mL fluorescein-labeled dextran (FITC-dextran, MW: 2×10^6; Sigma-Aldrich). Results of mouse CNV experiments [25] indicated that laser-induced CNV lesions were most active at 14 days after laser application and gradually self-resolved more than 28 days after the laser burn. This data was supported by our previous study of laser-burned monkey eyes [28].

We enucleated the eyes in the current study at 14 days after the CNV laser procedure, after euthanizing the animals per the previously described method. The eyes were removed and fixed for 30 minutes in 4% phosphate-buffered PFA. The cornea and lens were removed and the entire retina was carefully dissected from the eyecup. Radial cuts (4 to 6) were made from the edge to the equator, and the eyecup of the RPE-choroid-sclera (R-C-S) complex was flat mounted in Permalfuor (Beckman Coulter; Fullerton, CA, USA) with the scleral side facing down. Flat mounts were examined by fluorescence microscopy (Leica FW4000, Leica Microsystems Japan), and the total area of each CNV zone associated with each burn was measured. The CNV lesions were identified by the presence of fluorescent blood vessels on the choroidal/retinal interface circumscribed by a region lacking fluorescence. This process duplicated past reported procedures [33,34]. Two retinal specialists (HO and TA) and one non-specialist (NN) evaluated the size of the dextran-fluorescein perfused CNVs in a blinded manner, as described above.

Statistical Analyses

Analysis of variance (ANOVA) with Tukey's test was used to examine differences in the leakage and severity of the CNVs in the fluorescein angiograms and the area of the choroidal flat mount. Endothelial tube formation was also evaluated by this method. P-values less than 0.05 were considered significant.

Results

In Vitro Vasohibin-1 Release from the Device

Each result is shown as mean ± SD of three different experiments in Figure 1E. A prominent initial increase was observed in vasohibin-1 pellets (Pellet) and it appeared to almost plateau at 7 days after the start of incubation. A minor increase was observed in the vasohibin-1 delivery devices (VDD) with an almost level release observed over the 28 days of incubation. If we examine the amount released from the device (4×4×1.5 mm) between Days 7 and 28, the amount released was estimated to be 0.31 nM/day in the 10VDD group, 0.070 nM/day in the VDD group, 0.088 nM/day in the pellets, and 0 in the NVDD group (Fig. 1E) in a closed incubation system, when we used 500 mg/mL COLs for the permeable PEG/COLs membranes. These calculations were performed from the fitting line between 0 and 28 days. In rat experiments, the release amount would be less, because we used a smaller device for rats than used in the *in vitro* release assay. The larger device used in the *in vitro* release assay in Fig. 1E had 5.44 times (12.25 mm^2 vs 2.25 mm^2) larger drug-releasing surface area and 3.42 times faster releasing rate than that of the transplanted device used in rats, from the results of Fig. S1. The total amount of vasohibin-1 released from the 10VDD devices during the CNV suppression experiment in rats was estimated grossly to be approximately 4.28 nM over 2 weeks. The total amount of vasohibin-1 during the 2 weeks was estimated as about 14.6 nM from the results of Figure 1E, and was divided by 3.42, which is the difference in releasing rate between *in vitro* release assay and *in vivo* experiments, although the effective amount of vasohibin-1 in CNV suppression would be smaller than 4.28 nM, due to drug elimination from the eye. These results were confirmed by western blotting analysis; Figure 1D shows the representative results at Days 1, 7, 14, and 28. A greater amount of vasohibin-1 was observed in the 10VDD and pellet groups than was seen in the NVDD and VDD groups. The results of the pellet group at Day 1 (1d in Fig. 1D) was obtained after diluting the samples five times, because the concentration was too high to be shown by western blotting. However, the size of the pellets was much smaller after 7 days of incubation.

Endothelial Tube Formation

Endothelial tube formation of HUVECs cultured on the NHDF layer was assessed using anti-human CD31 immunostaining (Fig. 2). We used a range of native vasohibin-1 concentrations (from 0 to 10 nM, using 2 nM VEGF) for the preliminary experiments. After the initial examination, the cells were fixed and stained using anti-human CD31. Figures 2A–2G show representative photographs of the experimental results. Figure 2E shows the results of released vasohibin-1 (0.56 nM) from the devices with 2 nM VEGF. Figure 2H shows the average of each experiment; significantly fewer CD31-positive points were observed in released vasohibin-1-treated wells when compared to those of the vehicle released from the NVDD ($p = 0.000001$) or VEGF-treated control ($p = 0.000002$). Vasohibin-1 released from the device showed activity comparable to the native vasohibin-1.

Macro Examination

FD40 was detected in the device (Figs. S2A and S2B show color and fluorescein photographs, respectively) or in pellets (Figs. S2G and S2H) at the implant site through the conjunctiva in the live rats. When we enucleated the eyes at a week after device implantation, mild fibrosis was observed around the devices (Fig. S2C) and around the pellets (Fig. S2I). Fluorescein photography demonstrated the presence of FD40 in the device, with little fluorescein in the conjunctiva and surrounding tissues (Fig. S2D, arrow). FD40 was also detected in the sclera after removal of the device (Figs. S2E and S2F, arrow). Conversely, FD40 pellets showed strong fluorescein on the conjunctiva and surrounding tissues, as was seen for the pellet itself (Fig. S2J, arrow). Furthermore, little fluorescein was observed on the sclera after removal of the device (Figs. S2K and S2L, arrow). Similar conditions were observed when we examined the tissues at 2 weeks after device and pellet implantation; fluorescence was observed over a wider area for those specimens where the device was implanted compared to results at Week 1 (data not shown).

Immunohistology of Vasohibin-1

In immunostained eyes, vasohibin-1-positivity was found in only the 10VDD group (Fig. 3B), but not in the NVDD group (Fig. 3A) or the negative control without the first antibody (Fig. 3D), mainly at the region where vasohibin-1 releasing devices were placed. Pellets showed strong local immunoreactivity, but no immunoreactivity in the retina (Fig. 3C). Vasohibin-1 positivity was observed in the neural retina and optic nerve (white arrows in Fig. 3B). Strong immunoreactivity was observed in the choroid, RPE, and at the inner layer (such as the ganglion cell layer [GCL]) by magnified photographs after device implantation (Fig. 3E).

Leakage from CNV

Fluorescein angiography results of each group at 1 week after the laser CNV procedure are shown in Figure 4A. The results show that an intravitreal injection of vasohibin-1 on Day 4 after the CNV procedure led to a significant reduction of FA scores when compared to those of NVDD ($p = 0.00014$), pellet ($p = 0.020$), and vehicle injection ($p = 0.040$) (Fig. 4B). The 10VDD implantation led to a significant reduction of FA scores when compared to the result of the NVDD group ($p = 0.00006$). The VDD implantation led to a significant reduction of FA scores when compared to those of NVDD ($p = 0.000017$), pellet ($p = 0.012$), and vehicle injection ($p = 0.026$). Although FA scores of the 10VDD group seemed to be smaller than those of the pellet ($p = 0.065$) and vehicle injection ($p = 0.12$), the results were not significant. Figure 5A shows the FA results at Week 2 in each group. Significantly lower FA scores were observed for the vasohibin-1 intravitreal injection group when compared to those of NVDD ($p = 0.000022$), and vehicle intravitreal injection ($p = 0.0065$). Further, significantly lower FA scores were observed in the 10VDD group when compared to those of NVDD ($p = 0.000003$) and vehicle injection ($p = 0.0080$) (Fig. 5B). Significantly lower FA scores were also observed in the VDD group when compared to those of NVDD ($p = 0.000058$) and vehicle injection ($p = 0.011$).

Flat-mount Examination of the CNV Site

Choroidal flat mounts were prepared 2 weeks after device implantation; representative results of each group are shown in Figure 6A. The area of the CNV was 27,288±7,975 μm^2 for the NVDD group; 23,532±13,120 μm^2 for the VDD group; 17,382±715 μm^2 for the 10VDD group; 30,502±780 μm^2 for the vasohibin-pellet group; 26,900±9,067 μm^2 for the intravitreal vehicle injection group, and 12,731±4,113 μm^2 for the intravitreal vasohibin-1 injection group (Fig. 6B). The CNV area was smaller in eyes that were treated with 10VDD or intravitreal vasohibin-1 injection compared to the other treatments. A significantly smaller CNV area was observed in the 10VDD group when compared to those of the NVDD ($p = 0.0004$), pellet transplantation ($p = 0.0011$), and intravitreal vehicle injection groups ($p = 0.000015$). A significantly smaller CNV area was also